BeBeC-2018-D09

AN IMPROVED REGULARIZATION OF THE GENERALIZED INVERSE BEAMFORMING APPLIED TO A BENCHMARK DATABASE

Riccardo Zamponi[1] and Nicolas Van de Wyer[1] and Christophe Schram[1]
[1]von Karman Institute for Fluid Dynamics
Waterloosesteenweg 72, 1640, Sint-Genesius-Rode, Belgium

Abstract

Over recent years, inverse beamforming methods for acoustic source localization and source strength estimation have become increasingly considered in the aeroacoustic community. This is mainly due to their capability to accurately resolve coherent and distributed sources. In this paper a specific implementation of Generalized Inverse Beamforming (GIBF) technique, aimed at ensuring an accurate and robust source strength reconstruction, is presented. The paper discusses regularization approaches based on the Quasi-optimality criterion and the L-curve method for the determination of the optimized regularization parameters. The upgraded GIBF tool is applied to a benchmark dataset corresponding to a small-scale open-jet facility, the NASA Langley Quiet Flow Facility (QFF), for the characterization of airfoil self-noise. The source maps and the quantitative levels obtained for different integrated one-third octave band spectra are shown in comparison with a Conventional Beamforming (CB) technique. The results are also compared with data corresponding to different array analysis methods applied to the same test case. Finally, it is demonstrated that using a proper handling of the regularization process and the treatment of the background noise, GIBF can successfully resolve dominant aeroacoustic sources eliminating spurious ones.

1 INTRODUCTION

Inverse methods for the spatial localization and the strength estimation of acoustic sources have been widely and increasingly used for a great variety of aeroacoustic applications in the past decade. Indeed, the interpretation of aerodynamic noise sources is problematic because of their distributed and partially correlated nature and because of their radiation pattern that is usually not well defined. The Generalized Inverse Beamforming (GIBF), proposed by Suzuki [16], offers the possibility to solve these problems and to deal with coherent and incoherent, distributed

or compact multipole sources. This method is based on the eigenstructure of the microphone array cross-spectral matrix and considers the same array information and the same modeling of the source-receiver direct radiation used by Conventional Beamforming (CB) techniques. However, while direct beamforming methods (in addition to the above mentioned CB, this group includes deconvolution methods like CLEAN [8], DAMAS [4, 5] and their evolutions CLEAN-SC [15] and DAMAS2 [7]) deal with each source separately, assuming them to be uncorrelated, GIBF approaches the problem by considering all sources simultaneously, taking into account their effective correlation. The drawback of this approach is the mathematical implications linked to an inverse problem, which is most of the time ill-posed. For this reason, regularization strategies are required in order to allow an accurate strength reconstruction.

The purpose of this paper is to present an improved version of GIBF which ensures the characterization of complex aeroacoustic sources with a greater accuracy in the localization and a better estimation of the source strength. This is obtained by the use of automated methods for the definition of the optimized regularization parameters and of the stop criterion for the iteration count of the algorithm. A similar approach is adopted by Zavala [18, 19]. Subsequently, the code is applied to an experimental benchmark dataset corresponding to a small-scale open-jet facility, the NASA Langley Quiet Flow Facility (QFF) [1], and containing the leading/trailing edge noise measurements of a 2D airfoil. The results processed with GIBF are compared with the ones obtained by CB and with the ones presented by Bahr et al. [3]. These refer to several array analysis methods that are developed by different contributors and that are applied to the same test case. The application of GIBF to a benchmark database aims on one hand at validating the code and evaluating its performances and, on the other hand, showing the potentials and benefits of this method for complex applications. In this regard, the comparison between GIBF and other common beamforming techniques is of key importance.

The paper is structured as follows: the GIBF algorithm will be explained in Section 2, while the experimental setup considered for the validation will be illustrated in Section 3. Finally the main results and the comparisons between the different methods will be presented and discussed in Section 4 and 5.

2 ALGORITHM DESCRIPTION

The first step of the GIBF algorithm is the computation of the Cross Spectral Matrix ($\mathbf{C}$) from the recorded microphone signals. Since $\mathbf{C}$ is a non-negative definite and Hermitian matrix, it can be decomposed as:

$$\mathbf{C} = \mathbf{U}\Lambda\mathbf{U}^{\dagger} \tag{1}$$

where $\mathbf{U}$ is a unitary matrix containing orthonormal eigenvectors on its columns, Λ is a diagonal matrix consisting of their eigenvalues and $\mathbf{U}^{\dagger}$ is the complex conjugate transpose of $\mathbf{U}$. Each eigenvalue represents the overall strength related to a coherent sources distribution (under constraint of orthogonality) and the eigenvectors are associated to the sensors phase responses to these coherent sources distributions. It is then possible to define the *eigenmode* as the eigenvector including its magnitude:

$$\mathbf{v}_i = \sqrt{\lambda_i}\mathbf{u}_i \tag{2}$$

being $\mathbf{u}_i$ the i-th column vector of $\mathbf{U}$ and $\sqrt{\lambda_i}$ the corresponding eigenvalue.

The next step of the algorithm is to find the source distribution that recovers this eigenmode. Assuming that the superposition of the pre-defined sources at each grid point on the target domain produces an acoustic signal at the microphones as described by the eigenmodes, it is possible to express the mathematical relation:

$$\mathbf{v}_i = \mathbf{A}\mathbf{a}_i \tag{3}$$

where $\mathbf{a}_i$ is the i-th amplitude source vector and $\mathbf{A}$ is the $N_{grid} \times N_{mic}$ transfer matrix containing the source-receiver radiation patterns, N_{grid} being the number of grid points and N_{mic} the number of the microphones. This transfer function depends on the conditions under which the propagation happens. For example, if a monopole source is radiating in presence of a uniform open jet flow, the radiation pattern should be modified in order to consider the effect of the flow and the shear layer. A possible formulation for the transfer matrix between the microphone m and the grid point n to take a uniform flow of constant velocity into account can be described as [10]:

$$\{\mathbf{A}\}_{n,m} = \alpha_{n,m} \frac{r_{n,m}}{r_{c,m}} e^{j[(\mathbf{k}\cdot\mathbf{r}_{n,m}) + 2\pi f \Delta t_{n,m}]} \tag{4}$$

where $\mathbf{k}$ is the acoustic wave vector, $\mathbf{r}_{n,m}$ is the distance vector between the grid point and the microphone and f is the frequency at which the source is radiating. The corrections are calculated by the use of Snell's law in Amiet's method [2], adapted to a curved three-dimensional mean shear layer surface defined in the shear layer. $\alpha_{n,m}$ is the refraction amplitude correction while $\Delta t_{n,m}$ is the additional time (compared to a direct ray path with no flow) taken by an acoustic ray to travel from the grid point n to the microphone m due to the convection by the open jet flow and to the refraction by the shear layer. With the aim of normalizing the distance-related amplitude, $\alpha_{n,m}$ is multiplied by the ratio $r_{n,m}/r_{c,m}$, with c referring to the array center microphone.

The numerical problem of Eq. 3 is under-determined (the number of sources - *unknowns* - is greater than the number of microphones - *equations*) and ill-posed in Hadamard sense. Therefore it is common practice to find the minimum-norm solution of the problem addressed in Eq. 3 by either exploiting the Moore-Penrose inverse (since $N_{grid} \gg N_{mic}$ the right-inverse is used) or regularization strategies like the Tikhonov approach [17]. Tikhonov regularization modifies the original formulation of the problem by adding a residual norm term and a regularization parameter, μ, which balances the residual and solution norms, thus providing a solution like:

$$\mathbf{a}_i^* = argmin\{\|\mathbf{a}_i\|^2 + \mu^{-2}\|\mathbf{v}_i - \mathbf{A}\mathbf{a}_i\|^2\}. \tag{5}$$

An analytical solution of this minimization issue can be derived explicitly and is given by:

$$\mathbf{a}_i^* = \mathbf{A}^\dagger(\mathbf{A}\mathbf{A}^\dagger + \mu^2\mathbf{I})^{-1}\mathbf{v}_i \tag{6}$$

where $\mathbf{I}$ is the identity matrix.

It is possible to consider an arbitrary value for the regularization parameter or, as suggested by Suzuki [16], to define the μ value as a fraction of the maximum eigenvalue $\mu^2 = \varepsilon \max(eig(\mathbf{A}\mathbf{A}^\dagger))$, with ε typically ranging from 0.1% to 10%. However, as it has already been shown [6], the choice of the regularization strategy adopted for solving the inverse problem influences the results dramatically. Therefore, it is crucial, for GIBF, to select the optimal regularization factor at each step of the iterative process. For this reason, strategies based

on functions that correlate the solution norm and the residual norm in the Tikhonov problem are implemented in the code, following the approach described in [14]. These methods are the L-Curve, the Generalized Cross Validation (GCV) and the Quasi-optimality criterion. The first one computes the corner of log-log plot (which is usually a "L-shaped" curve) of the norm of a regularized solution versus the norm of the corresponding residual norm. The regularization parameter associated to the corner of the curve represents the trade-off between the size of a regularized solution and its fit to the given data. Both GCV and Quasi-optimality criterion are instead based on the minimization of two functions. For the first, the function that has to be minimized is (the subscript i is omitted for clarity):

$$\mathbf{G}(\mu) \equiv \frac{\|\mathbf{A}\mathbf{a}^* - \mathbf{v}\|^2}{(trace(\mathbf{I} - \mathbf{A}\mathbf{A}^I))^2} \tag{7}$$

where $\mathbf{A}^I$ is a matrix which produces the regularized solution $\mathbf{a}^*$ when multiplied with $\mathbf{v}$, i.e., $\mathbf{a}^* = \mathbf{A}^I\mathbf{v}$, while for the second:

$$\mathbf{Q}(\mu) \equiv \mu \left\| \frac{d\mathbf{a}^*}{d\mu} \right\|. \tag{8}$$

Under certain assumptions, both approaches correspond to finding a tradeoff between perturbation and regularization errors in the regularized solution $\mathbf{a}^*$. More information about the mathematical aspects of the three methods can be found in [14].

However, the use of the least-squares approach to find the minimum of the cost function causes source maps to blur [16]. Despite the $\mathscr{L}^2$ norm solution is certainly one of the exact solutions, except for the error associated with the regularization, the actual size of the source distribution is likely more compact for the majority of the applications. To increase the readability of the source map and to have a more accurate estimation of the overall strength of the source vector, the solution of the problem in Eq. 3 can be rewritten in terms of $\mathscr{L}^1$ norm:

$$\mathbf{a}_i^* = argmin\{|\mathbf{a}_i| + \mu^{-2}|\mathbf{v}_i - \mathbf{A}\mathbf{a}_i|^2\}. \tag{9}$$

This formulation excludes the possibility of an analytical solution, but an iterative approach such as the *Iteratively Reweighted Least Squares* (IRLS) algorithm [9] solves the issue. Starting from the regularized $\mathscr{L}^2$ solution retrieved by Eq. 6, the IRLS algorithm computes the amplitude source vector at the n^{th} iteration as:

$$\mathbf{a}_i^{n+1} = \mathbf{W}^{(n)}\mathbf{A}^\dagger(\mathbf{A}\mathbf{W}^{(n)}\mathbf{A}^\dagger + \mu^2\mathbf{I})^{-1}\mathbf{v}_i \tag{10}$$

where $\mathbf{W}^{(n)}$ is a diagonal matrix whose diagonal components w_i are given by $w_i = |a_i^{(n)}|$, a_i being the component of the vector $\mathbf{a}_i^*$ obtained by Eq. 6. The iteration process stops when the norm of the amplitude source vector starts increasing or the iteration counter reaches a pre-defined limit. For the choice of the value of μ in Eq. 9 and 10, the regularization strategies considered for the inverse problem with the $\mathscr{L}^2$ norm and referred to the standard Tikhonov approach cannot be applied since the $\mathscr{L}^1$ norm is minimized. In this case, with the aim of finding an optimized regularization parameter at each iteration of the algorithm, a generalization of L-curve method is considered and the solution and the residual $\mathscr{L}^1$ norms of the problem are evaluated in order to find the corner of the resulting log-log curve.

In both $\mathscr{L}^2$ norm and $\mathscr{L}^1$ norm formulations, an iterative approach is performed in order to guarantee the sparsity of the solution, minimize irregularities in the map and save computational time. During these iterations, the smallest components of the amplitude source vector are discarded on the basis of a reduction factor β ($0 < \beta < 1$). In this way, a reduced transfer matrix of size $(\beta N_{grid}) \times N_{mic}$ is obtained at each iteration. The algorithm stops when the amplitude source vector reaches a pre-defined size imposed by the user, which is chosen by the minimization of the cost function defined in Eq. 5 or in Eq. 9, depending on the considered norm.

3 EXPERIMENTAL SETUP

The benchmark test case considered for the validation of GIBF is labeled as NASA2 dataset [1] and contains data corresponding to leading/trailing edge noise measurements of a 2D airfoil immersed in a flow from the NASA Langley Quiet Flow Facility (QFF) open test section wind tunnel. An exhaustive description of the setup can be found in previous studies of trailing edge measurements [11] and in the original DAMAS [4] work.

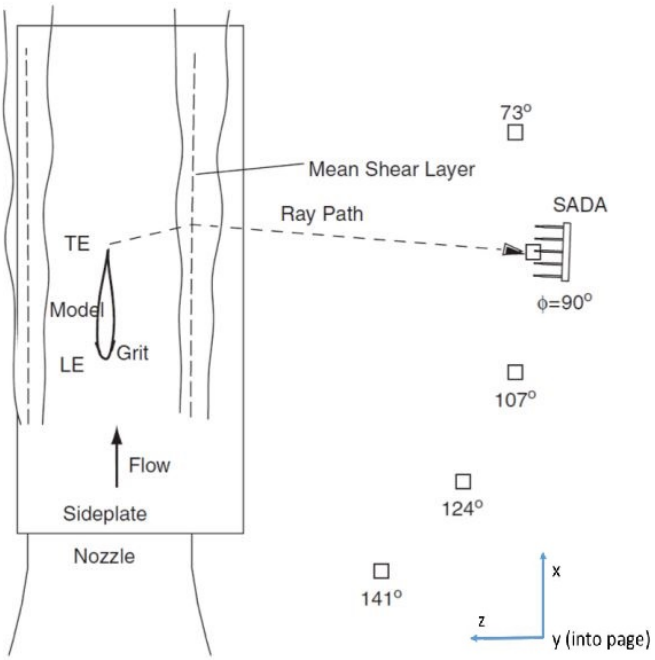

Figure 1: Setup for the Leading Edge/Trailing Edge measurements of the NACA 63-215 Mod-B full-span airfoil in NASA Langley QFF. The airfoil is installed in a clean configuration at its zero-lift angle of attack (-1.2°). The coordinate system origin is the center of the nozzle exit plane.

In Fig. 1 a scheme of the setup is shown. Particularly, a NACA 63-215 Mod-B full-span airfoil with a 0.406 m (16-inch) chord length and 0.914 m (36-inch) span is mounted at its zero-

lift angle of attack (-1.2°) relative to the vertical flow in the QFF. The model, installed in a clean configuration and therefore without the use of high-lift devices, presents a spanwise uniform sharp trailing edge of 0.127 mm (0.005-inch) thickness. Grid of size # 90 is distributed over the first 5 % of the leading edge of the model in order to ensure a fully turbulent boundary layer at the trailing edge. A 33-microphone Small Aperture Directional Array (SADA) is positioned at an elevation angle of 90° with respect to the pressure side of the model. Data are acquired with the SADA at a free stream Mach number of 0.17 and at a total temperature of 26.35° C. The sampling rate for the signal is 142,857.71 Hz, and a total of 2,048,000 samples are recorded simultaneously for all microphone channels, corresponding to an acquisition time of 14.3 s.

Considering the zero-lift condition of the model and its orientation in the facility, it is possible to assume that the mean shear layer bounding the flow remains planar and attached to the nozzle lip line and that it is located at a constant distance (0.305 m) from the centerline of the nozzle. The model itself is offset from the tunnel centerline by 0.133 m, and the SADA is located 1.524 m from the model trailing edge. With the aim of studying the corresponding background noise, data with the model removed from the facility are acquired using the SADA at the same position of the first acquisition.

4 SOURCE LOCALIZATION

In this section a qualitative study based on the comparison of the source maps processed on a one-third octave band basis is presented. Since the airfoil is installed in a clean configuration, the noise sources are expected at the model trailing edge and leading edge regions. The capability of the algorithm to isolate and correctly resolve those distributed sources is evaluated.

The first part of this qualitative analysis shows a comparison between the results obtained with CB and the ones obtained with GIBF. For both of them, the array outputs are presented for four one-third octave frequencies, 3.15, 8, 12.5 and 20 kHz, in analogy with the work carried out by Brooks and Humphreys [4] on the same test case. The displayed results are obtained by summing the individual frequency contributions processed for each band. A planar square scanning grid of 1.27 m per side is placed through the chordline at 1.524 m from the SADA array and extends beyond the side-plates that hold the airfoil and that represent reflecting elements. Each side of the grid presents 51 points corresponding to 51 potential sources, for a total of 2601 points and a spatial resolution of the grid of 2.54 cm. For both methods, the diagonal removal of the cross spectral matrix [12] is applied with the aim of reducing the microphone self noise, while the background noise is handled by subtracting the cross spectral matrix corresponding to the acquisition without the model from the original one. Finally, no shading algorithms are used for the processing of the data, despite the fact that NASA2 benchmark provides the frequency dependent weight for each microphone.

In Fig. 2 the source maps obtained for the CB are shown. The vertical black lines at $y = \pm$ 0.46 m indicate the test section side-walls, whereas the horizontal ones at $x = 0.6$ m and $x =$ 1 m indicate respectively leading edge and trailing edge of the model. In each figure the flow goes from the bottom to the top. Concerning the output of the map expressed in term of source strength, a dynamic range of 10 dB is used for CB.

As it is possible to notice from the maps, there is a shift for the concentration of the most intense source regions from the trailing edge to the leading edge with the increasing frequency.

For $f_{1/3}$ = 3.15 kHz (Fig. 2a) the main source is placed downstream of the trailing edge.

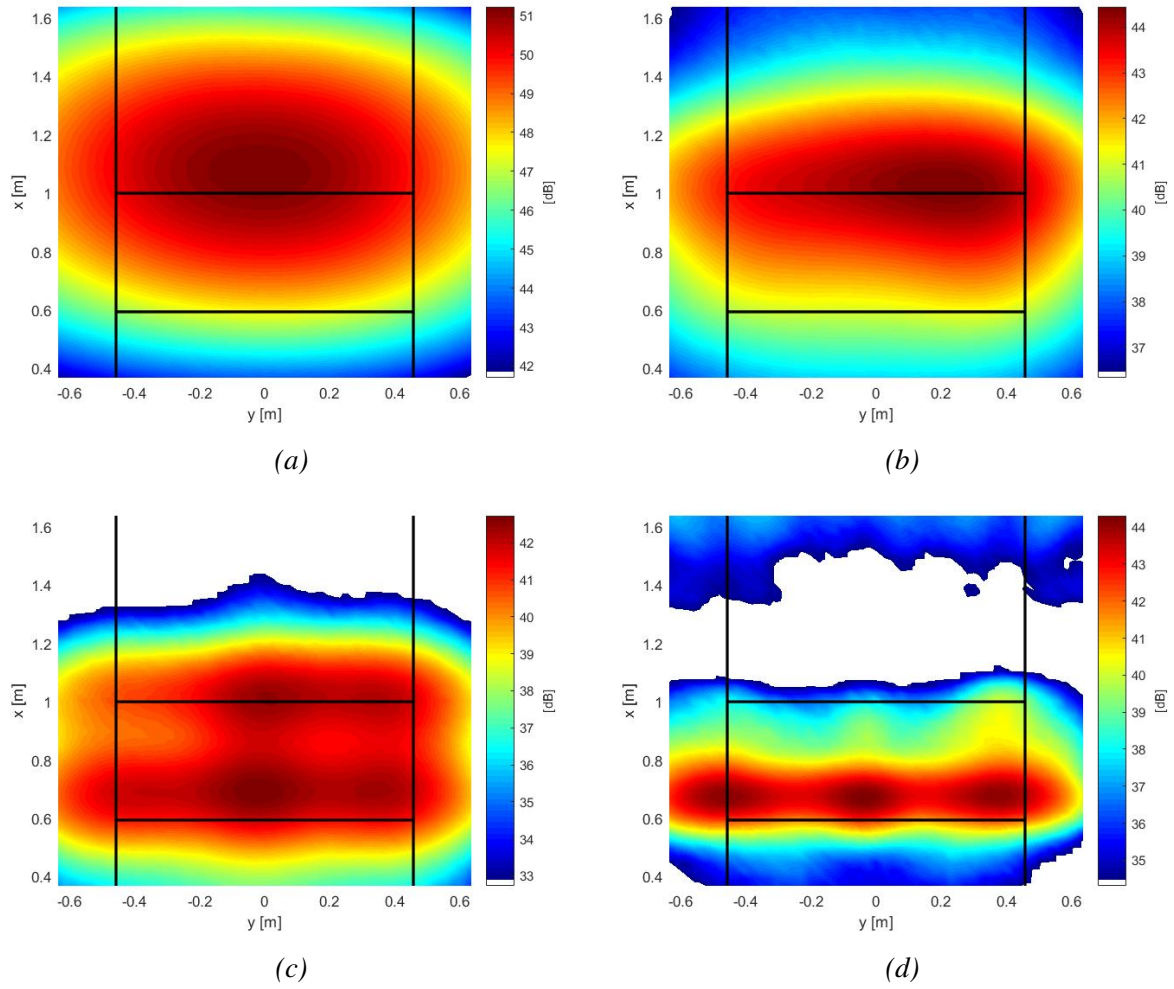

Figure 2: CB source maps for the NACA 63-215 Mod-B full-span airfoil. The vertical black lines indicate the test section side-walls, the horizontal ones indicate leading edge and trailing edge of the model. The flow goes from the bottom to the top of the map. The one-third octave frequencies are: (a) 3.15 kHz, (b) 8 kHz, (c) 12.5 kHz and (d) 20 kHz. The dynamic range of the maps is 10 dB.

However, the dynamic range of the map is low, showing a difference between the leading and the trailing edge regions lower than 3 dB. For this one-third octave band, CB is not able to isolate properly the source because of the frequency-dependent beamwidth characteristics of the antenna. Indeed, the SADA array has been designed to have a 30,48 cm (1 ft.) main lobe at 10 kHz, so at frequencies less than half of that, the separation of multiple source contributions is problematic. For $f_{1/3}$ = 8 kHz (Fig. 2b) the sources are concentrated along the trailing edge and, as expected, the spatial resolution of the map increases because of the higher frequency. For $f_{1/3}$ = 12.5 kHz (Fig. 2c) the map shows a significant energy level in both the leading edge and trailing edge source regions. The CB is able to localize the contributions of these sources and to separate them, but the dynamic range should be further reduced in order to visualize this

separation. Finally, for $f_{1/3}$ = 20 kHz (Fig. 2d), the sources are clearly disposed on the leading edge and concentrated in three spots, in the middle and in proximity of the external borders of the profile.

In this configuration, the noise is reflected on the two side-walls. Since their presence is not taken into account in the transfer matrix, the reflected sources are interpreted by the CB method as artefacts located in the regions beyond $\pm$ 0.46 m.

In Fig. 3 the GIBF results corresponding to the same cases of Fig. 2 are presented. For the Tikhonov regularization process the Quasi-optimality criterion has been used to retrieve the optimized value of μ (see Sec. 2). This choice is related to the better response of this method in the treatment of distributed sources with respect to the other methods, as it will be shown later. Similarly, since the norm $\mathscr{L}^1$ is then minimized, an optimized value of μ for the IRLS algorithm is obtained at each iteration by evaluating the corner of a "pseudo L-curve" correlating solution and residual $\mathscr{L}^1$ norms. Concerning the stop criterion for the iteration count, the resolution of the source localization increases with the number of iterations of the algorithm. On the other hand, if relevant sources risk to be discarded, a compromise between the readability of the map and the loss of information has to be found. The determination of the proper stop criterion is made a posteriori following a first run of the algorithm. From this first run, the cost function of Eq. 9 is evaluated and the iteration counter corresponding to its minimum is chosen for the second and definitive run of the code. For the presentation of the results, the same settings of the CB maps are considered except for the dynamic range, that is risen to 20 dB.

All the GIBF resulting maps present an important improvement of the readability and a significant reduction of the spurious sources. Because of the inverse nature of the problem, it is not possible to relate the source strength peak level obtained by this technique to the peaks of CB maps. Moreover, this level depends also on the number of iterations of the algorithm. An additional scaling factor is therefore required to compare the integrated spectra obtained in the quantitative analysis.

For $f_{1/3}$ = 3.15 kHz (Fig. 3a) the source distribution significantly differs from the one obtained with CB. The position of the main lobe is displaced downwards at the trailing edge level and the sources appear to be concentrated around the center of the trailing edge. A deeper analysis of the case with the purpose of understanding the discrepancy between CB and GIBF maps should be performed. For $f_{1/3}$ = 8 kHz (Fig. 3b) the distributed sources along the trailing edge line are well defined and present a uniform distribution. Moreover, contrary to the CB case, sources along the leading edge can be detected and a discrepancy of about 10 dB between these two regions can be observed. For $f_{1/3}$ = 12.5 kHz (Fig. 3c) the leading edge and trailing edge sources are visually well separated and present a similar level of source strength. The sources are homogeneously distributed and for the leading edge it is possible to identify the same three peaks of the related CB map. Furthermore, the sources extend also beyond the side-plates, especially for $y < -0.46$ m for both leading and trailing edge. This is probably due to the influence of the acoustic reflection of the walls. Additional sources are also detected in the lower boundary of the map. Most likely, they represent artifacts generated by numerical issues. For $f_{1/3}$ = 20 kHz (Fig. 3d), the algorithm is able to provide a uniform and clean visualization of the distributed sources along the leading edge, without the presence of spurious ones. Like in the previous case, the sources extend also beyond the side-plates, particularly for $y < -0.46$ m.

The second part of the qualitative analysis aims at showing the influence in terms of source visualization of the right choice of the regularization strategy for the computation of the initial

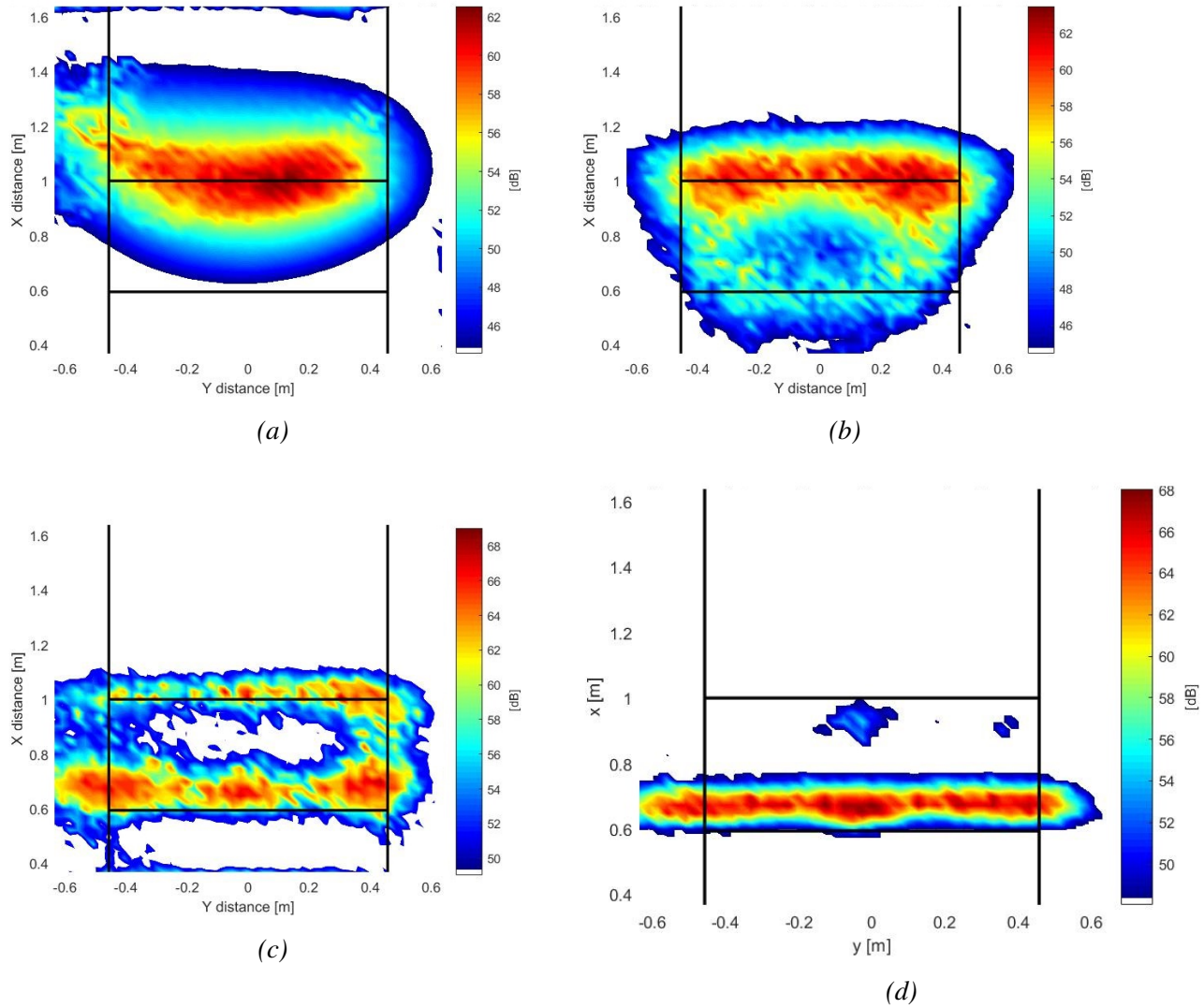

Figure 3: GIBF source maps for the NACA 63-215 Mod-B full-span airfoil. The one-third octave frequencies are: (a) 3.15 kHz, (b) 8 kHz, (c) 12.5 kHz and (d) 20 kHz. The algorithm is based on the Quasi-optimality criterion for the determination of the optimized regularization parameter in Tikhonov solution and on the minimization of $\mathscr{L}^1$ norm. The optimized value of the regulation parameter in the IRLS algorithm is determined by evaluating the corner of a "pseudo L-curve" correlating solution and residual $\mathscr{L}^1$ norm. The dynamic range of the maps is 20 dB.

source amplitude. In Fig. 4 a comparison between source maps obtained with the different regularization methods implemented in the algorithm is depicted. The maps refer to the one-third octave frequency 12.5 kHz, which will be of core importance in the following part of the paper. In the presented analysis, in order to emphasize the differences between the source maps, the IRLS algorithm has not been used and the minimization of the norm $\mathscr{L}^2$ has been considered. Suzuki's method has been adopted in Fig. 4a, 4b and 4c with three different values for ε (i.e.

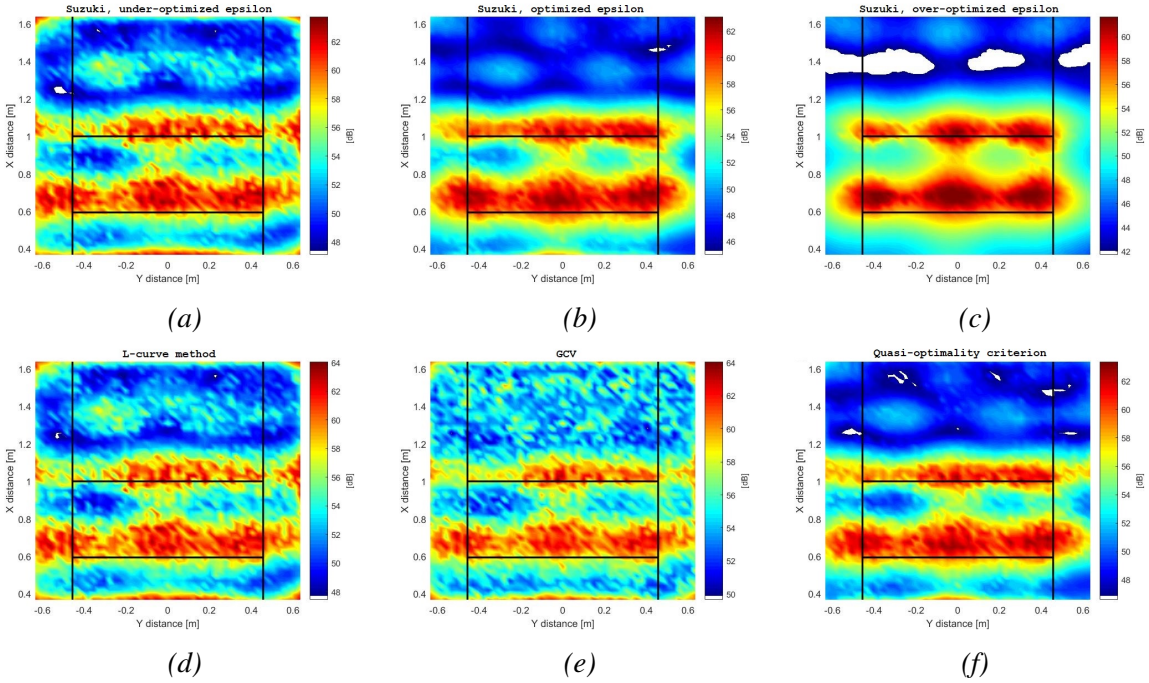

Figure 4: GIBF source maps comparison of the different regularization methods implemented in the algorithm: (a) Suzuki, under-optimized value of ε, (b) Suzuki, optimized value of ε, (c) Suzuki, over-optimized value of ε, (d) L-curve method, (e) GCV and (f) Quasi-optimality criterion. The one-third octave frequency is 12.5 kHz. In order to emphasize the differences between the methods, the norm $\mathscr{L}^2$ is minimized. The dynamic range of the maps is 20 dB.

the fraction of the maximum eigenvalue) corresponding respectively to an under-optimized, an optimized and an over-optimized situation. The optimized fraction of the greatest eigenvalue ε (4b) has been chosen in accordance to the qualitative results obtained with DAMAS algorithm applied to the same test case [3, 4]. Deviations from this value bring to errors in the source visualization. Indeed, when the regularization parameter μ is too low (Fig. 4a), the solution of the inverse problem is still very sensitive to perturbations and this causes the generation of artefacts in the boundaries that do not reflect the effective source distribution. When instead the regularization parameter is excessive (Fig. 4c), the solution of the inverse problem is too smooth and the sources appear to be concentrated in spots. This does not reflect the effective distribution neither. In Fig. 4d, Fig. 4e and Fig. 4f, the performances of respectively the L-curve method, the GCV and the Quasi-optimality criterion for the automatic choice of the optimized regularization parameter are evaluated. From a qualitative point of view, L-curve method and GCV tend to underestimate μ, leading to source maps similar to the one in Fig. 4a. On the other hand, Quasi-optimality criterion is able to retrieve a regularization parameter close to the optimized one, justifying the choice of its exploitation for the post-processing of NASA2 benchmark data, as already mentioned.

Finally, the third and last part of the qualitative analysis presents a comparison between the maps obtained with GIBF and the results published by Bahr et al. [3] (Fig. 5). The contributions

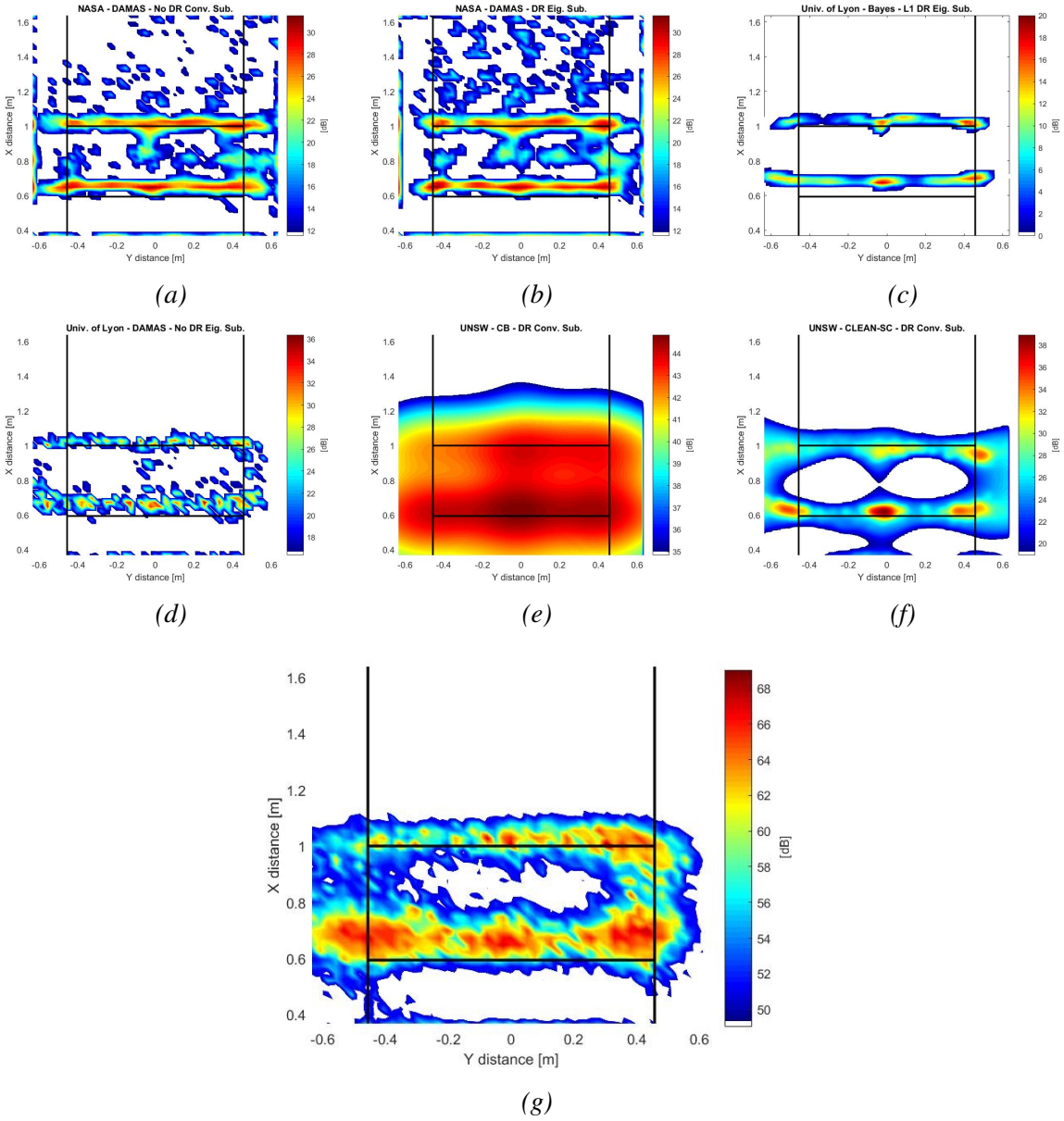

Figure 5: Qualitative comparison of the NASA2 benchmark contributions corresponding to a one-third octave frequency of 12.5 kHz. The algorithms used for the source maps are: (a) DAMAS, from NASA (no DR, conventional subtraction), (b) DAMAS, from NASA (DR, eigenvalue subtraction), (c) Bayesian reconstruction, from University of Lyon (DR, eigenvalue subtraction), (d) DAMAS, from University of Lyon (no DR, eigenvalue subtraction), (e) CB, from UNSW (DR, conventional subtraction) and (f) CLEAN-SC, from UNSW (DR, conventional subtraction). In (g) the source map computed by GIBF is shown again. All maps aside from (e) are set to a 20 dB dynamic range.

for the NASA2 benchmark case come from three organizations: NASA Langley Research Center (using DAMAS), University of Lyon (using Sparse Bayesian Reconstruction[1] and DAMAS) and University of New South Wales (using CB and CLEAN-SC). All the contributors processed the data corresponding to $f_{1/3}$ = 12.5 kHz. This choice is related to the similar energetic levels of the leading edge and trailing edge sources and, therefore, to the possibility to assess the performances of each code in terms of source isolation. Due to the experimental nature of the measurements, it is important to point out that the real source distribution is still not known with certainty. Sources are expected to occur just downstream of the leading edge and at the trailing edge of the airfoil. Both are expected to have distributed characteristics, while the source strengths are unknown.

As it is possible to notice, all the methods are able to successfully isolate the source regions. The focus points of the comparison with GIBF can be expressed as follows:

- For CLEAN-SC (Fig. 5f) the acoustic source energy in the map appears to be concentrated in isolated spots along the leading edge and the trailing edge and do not properly express the expected distributed nature of leading edge and trailing edge regions. GIBF shows source characteristics closer to the distributed ones and does not present artefacts at the lateral boundaries of the map.

- Bayesian reconstruction (Fig. 5c) presents a better spatial resolution than GIBF and a total absence of spurious sources at the boundaries of the map. However, the source distribution is still more irregular with a concentration of energy near the model center span and the side-walls. Thus, conclusions similar to the ones for CLEAN-SC case can be drawn.

- The source distribution processed by DAMAS (Fig. 5a, Fig. 5b and Fig. 5d) is closer to the expected one and it presents a better spatial resolution than GIBF in the source regions. However, for this algorithm, implementation plays a strong role in the distribution of low-level spurious sources. In NASA's results, for example, the effective sources are homogeneously distributed along the leading and trailing edge with no significant difference for the SPL. Nevertheless, the maps appear less readable and there are artefacts at the boundaries of the scanning grids. These are probably due to edge effects for the presence of sources outside the scanning grid [4]. The DAMAS source maps from University of Lyon are instead cleaner and do not present artefacts at the lateral boundaries. Nevertheless, the source distribution results discontinuous with isolated peaks along the leading and the trailing edge.

- The comparison with CB (Fig. 5e) has already been discussed in the previous section.

In Section 5 the discussion will be extended to the quantitative analysis.

5 INTEGRATED SOURCE SPECTRA

This section concerns the quantitative estimation of the integrated power spectra of the leading edge and trailing edge regions computed at the center of the array. Following the approach used

[1] Informations about this inverse method can be found in [13].

by Brooks and Humphreys in the original DAMAS [4] work, the one-third octave band spectra are determined by summing the pressure-squared values of each scanning grid point within rectangular boxes surrounding the leading and trailing edge regions. A visual representation of the integration areas is shown in Fig. 6a. The dimensions of the one for the leading edge are 812.8 mm x 279.3, while the one for the trailing edge are 812.8 mm x 406.1 mm. As the region's spanwise length is 2.5 ft, the sums are divided by 2.5 in order to put the spectral results on a per foot basis and therefore to allow the comparison with the published data.

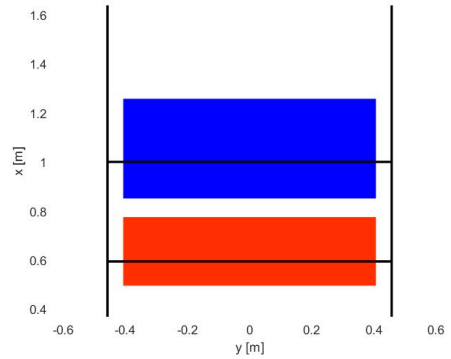

(a)

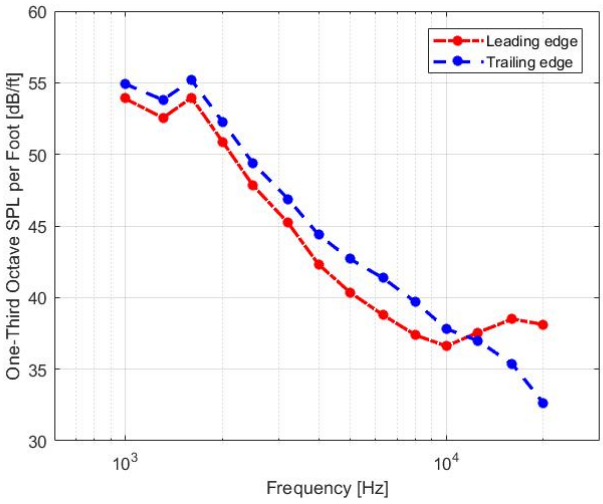

(b)

Figure 6: Quantitative analysis of the leading edge and trailing edge regions of the model. In (a) the areas considered for the integration are shown. In (b) the integrated one-third octave spectra per foot span computed with CB are presented.

In Fig. 6b it is possible to analyze the one-third octave spectra curves processed by CB. From the analysis of the behaviour of the curves, the trailing edge noise appears to be dominant for frequencies up to 11 kHz, after which the leading edge one prevails. This trend is shown also by the source maps in Fig.2 and Fig. 3. Anyway, especially at low frequencies, the leading edge noise results contaminated by the trailing edge one because of the beamwidth characteristics of the antenna, as already explained above. This is expressed by the fact that the behaviour of the integrated leading edge spectra follows the one of the integrated trailing edge spectra. The use of more performing algorithms makes it possible to solve this problem and to determine a better and more reliable estimation of the source strengths.

In Fig. 7 the integrated one-third octave band spectra per-foot-span referred to the leading edge area and computed by the different analysis methods already presented and by GIBF are shown. A scaling factor is applied to GIBF in order to retrieve the proper SPL. This has been determined by confronting the SPL of the integrated one-third octave band spectra of CB and GIBF for a simulated test case. A method to estimate a more accurate scaling factor is currently under development. All the leading edge spectra present a similar behaviour between 6 kHz and 20 kHz[2], suggesting that the differences in the qualitative maps at 12.5 kHz analyzed in

[2]The divergence of CB has already been discussed in the previous paragraph.

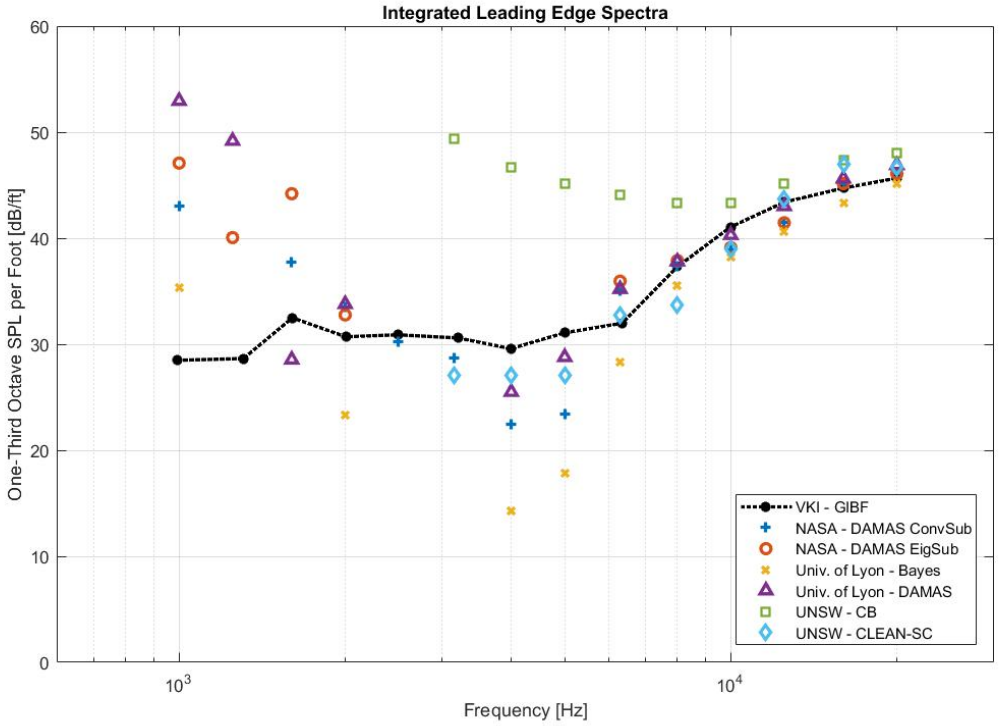

Figure 7: Integrated leading edge one-third octave band spectra per-foot-span computed from various analysis methods.

the previous section tend to average out within the integration procedure. In this range of frequencies, GIBF follows successfully the trend of the other methods. Below approximately 6 kHz, the advanced techniques start showing a significant divergence in both spectral level and shape and the SPL computed is not reliable anymore. Thus, for lower frequencies, the integrated leading edge one-third octave band spectra do not represent a proper validation test case for the source strength estimation by GIBF. As stated by Bahr et al. [3], one of the reason of this limitation can be related to the microphone antenna used for the measurement. Because of the frequency-dependent beamwidth characteristics of the SADA array, separating multiple source contributions at frequencies less than 5 kHz may be difficult even for advanced methods.

The integrated one-third octave band spectra per-foot-span referred to the trailing edge are instead presented in Fig. 8. The spectra computed by the other advanced methods show a more uniform behaviour in relationship to the leading edge spectra for the low frequencies, most probably because of the dominance of the trailing edge noise over the leading edge noise in this range. Indeed, the calculation of the integrated level of the dominant sources at low frequencies presents less variability with respect to array resolution when compared to the level of a weaker source [3]. This observation is reinforced by the increased variability between the different beamforming techniques that the trailing edge spectra show in the frequency range where the leading edge noise results to be dominant. However, despite the qualitative agreement between the advanced methods, for frequencies lower than 4 kHz, GIBF diverges from the rest of the predictions, and the divergence becomes particularly significant at 1.6 kHz, spanning well over

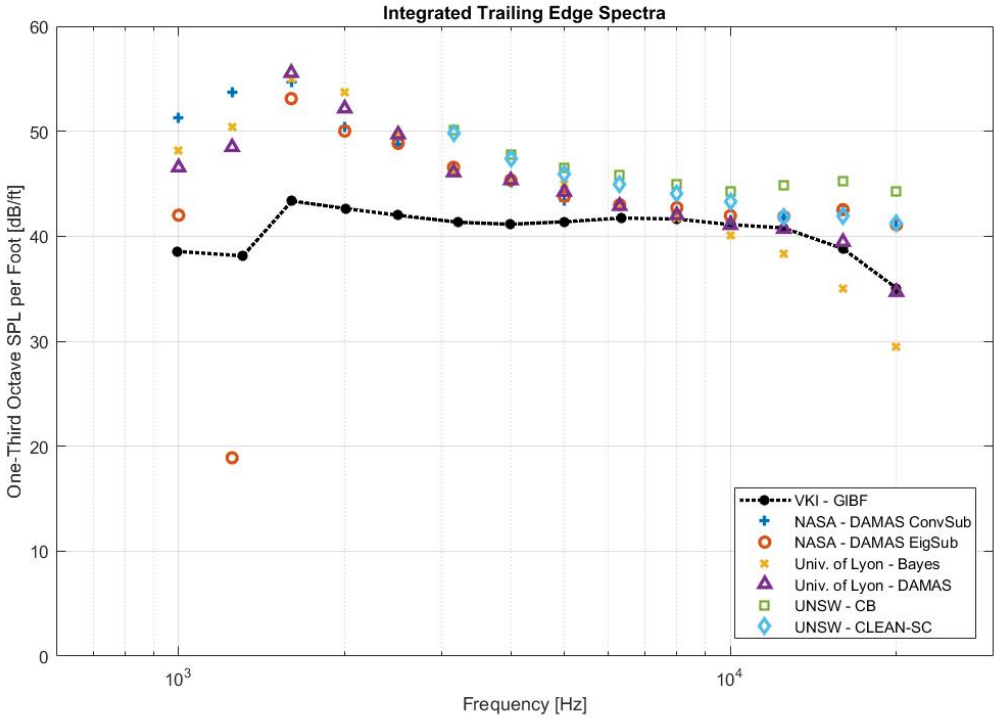

Figure 8: Integrated trailing edge one-third octave band spectra per-foot-span computed from various analysis methods.

10 dB. The causes of this behaviour are still under investigation. A possible reason may be the presence of sources outside the scanning grid (e.g. at the nozzle outlet) at the considered range of frequencies. This leads to a concentration of acoustic energy at the boundaries of the map and to a significant underestimation of the SPL in the trailing edge integration area. More studies will be performed in the near future in order to better understand the phenomenon.

6 CONCLUSION

An improved version of the Generalized Inverse Beamforming (GIBF) is developed and implemented with the aim of efficiently characterizing complex aeroacoustic sources. The use of automated methods for the determination of the regularization parameters of the algorithm turns out to be essential for an accurate localization of the distributed sources and for an estimation of their strength.

The results presented in the paper show that GIBF can be considered a valid tool for the spatial localization of aeroacoustic distributed sources. The code is applied to NASA2 benchmark dataset and confronted with other advanced techniques applied to the same data. The computation with the GIBF provides a distribution of the sources along the leading edge and trailing edge regions in agreement with the previous studies conducted on the test case. Two different kinds of analysis are performed, a qualitative one and a quantitative one. From the qualitative point of view, four one-third octave band frequencies are evaluated. GIBF shows significant

improvements in terms of visualization of the sources compared with Conventional Beamforming (CB). For the 12.5 kHz band, an extensive comparison with the other advanced methods is carried out. In this case, the source distribution computed by GIBF is closer to the expected distribution at the airfoil trailing edge and leading edge than the ones computed by the majority of the other algorithms, without the presence of spurious sources outside the model region. In addition, the dataset is used also to perform an analysis of the different regularization strategies implemented in the algorithm, justifying the choice of the Quasi-optimality criterion as regularization method. Concerning the quantitative comparison, the integrated one-third octave band spectra of the leading edge and trailing edge regions are evaluated. While for high frequencies GIBF is able to provide results consistent with the predictions of the other methods, for low frequencies it presents an underestimation of the SPL, especially for the trailing edge noise. This issue is currently under investigation and may depend on the presence of sources outside the scanning grid for the considered range of frequencies.

7 ACKNOWLEDGMENTS

This project has received funding from the European Union's Horizon 2020 research and innovation program under the Marie Skłodowska-Curie grant agreement No 722401.

REFERENCES

[1] "Arraybenchmark : Fachgebiet Technische Akustik - BTU Cottbus-Senftenberg - URL: https://www.b-tu.de/fg-akustik/lehre/aktuelles/arraybenchmark."

[2] R. K. Amiet. "Refraction of sound by a shear layer." *Journal of Sound and Vibration*, 58(4), 467–482, 1978.

[3] C. J. Bahr, W. M. Humphreys, D. Ernst, T. Ahlefeldt, C. Spehr, A. Pereira, Q. Leclère, C. Picard, R. Porteous, D. Moreau, J. R. Fischer, and C. J. Doolan. "A Comparison of Microphone Phased Array Methods Applied to the Study of Airframe Noise in Wind Tunnel Testing." In *23rd AIAA/CEAS Aeroacoustics Conference*. American Institute of Aeronautics and Astronautics.

[4] T. F. Brooks and W. M. Humphreys. "A deconvolution approach for the mapping of acoustic sources (DAMAS) determined from phased microphone arrays." *Journal of Sound and Vibration*, 294(4-5), 856–879, 2006.

[5] T. F. Brooks and W. M. Humphreys. "Extension of DAMAS phased array processing for spatial coherence determination (DAMAS-C)." *AIAA paper*, 2654, 2006, 2006.

[6] C. Colangeli, P. Chiariotti, and K. Janssens. "Uncorrelated noise sources separation using inverse beamforming." In *Experimental Techniques, Rotating Machinery, and Acoustics, Volume 8*, pages 59–70. Springer, 2015.

[7] R. P. Dougherty. "Extensions of DAMAS and benefits and limitations of deconvolution in beamforming." *AIAA paper*, 2961(11), 2005.

[8] J. A. Högbom. "Aperture Synthesis with a Non-Regular Distribution of Interferometer Baselines." *Astron. Astrophys. Suppl. Ser.*, 15, 417–426, 1974.

[9] P. J. Huber. "Robust statistics." *Wiley Series in Probability and Statistics, John Wiley & Sons*, 1981.

[10] W. M. Humphreys Jr, T. F. Brooks, W. W. Hunter Jr, and K. R. Meadows. "Design and use of Microphone Directional Arrays for Aeroacoustic Measurements." 1998.

[11] F. V. Hutcheson and T. F. Brooks. "Measurement of trailing edge noise using directional array and coherent output power methods." *International Journal of Aeroacoustics*, 1(4), 329–353, 2002.

[12] F. V. Hutcheson and T. F. Brooks. "Effects of angle of attack and velocity on trailing edge noise determined using microphone array measurements." *International Journal of Aeroacoustics*, 5(1), 39–66, 2006.

[13] A. Pereira, J. Antoni, and Q. Leclère. "Empirical Bayesian regularization of the inverse acoustic problem." *Applied Acoustics*, 97, 11–29, 2015.

[14] A. Rieder. "On the regularization of nonlinear ill-posed problems via inexact Newton iterations." *Inverse Problems*, 15(1), 309, 1999.

[15] P. Sijtsma. "CLEAN based on spatial source coherence: AIAA Paper 2007-3436[NLR-TP-2007-345]." *NLR Technical Reports*, 2007.

[16] T. Suzuki. "L1 generalized inverse beam-forming algorithm resolving coherent/incoherent, distributed and multipole sources." *Journal of Sound and Vibration*, 330(24), 5835–5851, 2011.

[17] R. Willoughby. "Solutions of Ill-Posed Problems (A. N. Tikhonov and V. Y. Arsenin)." *SIAM Review*, 21(2), 266–267, 1979.

[18] P. Zavala, W. De Roeck, K. Janssens, J. Arruda, P. Sas, and W. Desmet. "Generalized inverse beamforming with optimized regularization strategy." *Mechanical Systems and Signal Processing*, 25(3), 928–939, 2011.

[19] P. A. Zavala, W. De Roeck, K. Janssens, J. R. Arruda, P. Sas, and W. Desmet. "Monopole and dipole identification using generalized inverse beamforming." *AIAA Paper*, 3740, 2010.